



**TEST MECHANISM FOR MEASURING PITCH-DAMPING
DERIVATIVES OF MISSILE CONFIGURATIONS AT
HIGH ANGLES OF ATTACK**

**Bob L. Uselton and James C. Uselton
ARO, Inc.**

**VON KÁRMÁN GAS DYNAMICS FACILITY
ARNOLD ENGINEERING DEVELOPMENT CENTER
AIR FORCE SYSTEMS COMMAND
ARNOLD AIR FORCE STATION, TENNESSEE 37389**

May 1975

Final Report for December 19, 1974

Approved for public release; distribution unlimited

Prepared for

**DIRECTORATE OF TECHNOLOGY
ARNOLD ENGINEERING DEVELOPMENT CENTER
ARNOLD AIR FORCE STATION, TENNESSEE 37389**

NOTICES

When U. S. Government drawings specifications, or other data are used for any purpose other than a definitely related Government procurement operation, the Government thereby incurs no responsibility nor any obligation whatsoever, and the fact that the Government may have formulated, furnished, or in any way supplied the said drawings, specifications, or other data, is not to be regarded by implication or otherwise, or in any manner licensing the holder or any other person or corporation, or conveying any rights or permission to manufacture, use, or sell any patented invention that may in any way be related thereto.

Qualified users may obtain copies of this report from the Defense Documentation Center.

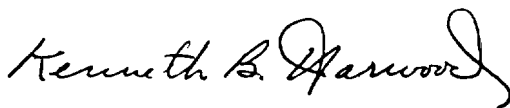
References to named commercial products in this report are not to be considered in any sense as an endorsement of the product by the United States Air Force or the Government.

This report has been reviewed by the Information Office (OI) and is releasable to the National Technical Information Service (NTIS). At NTIS, it will be available to the general public, including foreign nations.

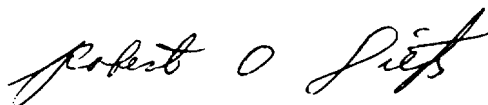
APPROVAL STATEMENT

This technical report has been reviewed and is approved for publication.

FOR THE COMMANDER



KENNETH B. HARWOOD
Captain, CF
Research and Development
Division
Directorate of Technology



ROBERT O. DIETZ
Director of Technology

UNCLASSIFIED

| REPORT DOCUMENTATION PAGE | | READ INSTRUCTIONS BEFORE COMPLETING FORM |
|--|--|---|
| 1. REPORT NUMBER AEDC-TR-75-43 | 2. GOVT ACCESSION NO. | 3. RECIPIENT'S CATALOG NUMBER |
| 4. TITLE (and Subtitle) TEST MECHANISM FOR MEASURING PITCH-DAMPING DERIVATIVES OF MISSILE CONFIGURATIONS AT HIGH ANGLES OF ATTACK | 5. TYPE OF REPORT & PERIOD COVERED Final Report, Dec 19, 1974 | |
| | 6. PERFORMING ORG. REPORT NUMBER | |
| 7. AUTHOR(s) Bob L. Uselton and James C. Uselton, ARO, Inc. | 8. CONTRACT OR GRANT NUMBER(s) | |
| 9. PERFORMING ORGANIZATION NAME AND ADDRESS Arnold Engineering Development Center Arnold Air Force Station, TN 37389 | 10. PROGRAM ELEMENT, PROJECT, TASK AREA & WORK UNIT NUMBERS Program Element 65807F | |
| 11. CONTROLLING OFFICE NAME AND ADDRESS Arnold Engineering Development Center (DYFS), Arnold Air Force Station, TN 37389 | 12. REPORT DATE May 1975 | |
| | 13. NUMBER OF PAGES 30 | |
| 14. MONITORING AGENCY NAME & ADDRESS (if different from Controlling Office) | 15. SECURITY CLASS. (of this report) UNCLASSIFIED | |
| | 15a. DECLASSIFICATION/DOWNGRADING SCHEDULE N/A | |
| 16. DISTRIBUTION STATEMENT (of this Report) Approved for public release; distribution unlimited. | | |
| 17. DISTRIBUTION STATEMENT (of the abstract entered in Block 20, if different from Report) | | |
| 18. SUPPLEMENTARY NOTES Available in DDC. | | |
| 19. KEY WORDS (Continue on reverse side if necessary and identify by block number) <div style="display: flex; justify-content: space-between;"> <div style="width: 30%;"> aerodynamics missiles angle of attack supersonic flow </div> <div style="width: 30%;"> dynamic tests dynamics stability damping </div> <div style="width: 30%;"> pitch (motion) </div> </div> | | |
| 20. ABSTRACT (Continue on reverse side if necessary and identify by block number) <p>Pitch-damping tests were conducted at $M_\infty = 1.96$ to evaluate the newly developed high-alpha missile test mechanism. Data were obtained utilizing the small-amplitude free-oscillation technique at angles of attack from -12 to 86 deg at Reynolds numbers, based on model diameter, of 0.086×10^6 and 0.187×10^6. Two missile configurations having length-to-diameter ratios (l/d) of 10 and 15 were tested. The $l/d = 10$ configuration is commonly known as</p> | | |

UNCLASSIFIED

UNCLASSIFIED

20, Continued

the Basic Finner. The test mechanism proved capable of measuring the pitch derivatives. Strut interference was not appreciable. The derivatives were found to be nonlinear functions of angle of attack, and previously published data at low angles of attack agreed well with the present results.

UNCLASSIFIED

PREFACE

The work reported herein was conducted by the Arnold Engineering Development Center (AEDC), Air Force Systems Command (AFSC), Arnold Air Force Station, Tennessee, under Program Element 65807F. The results presented were obtained by ARO, Inc. (a subsidiary of Sverdrup & Parcel and Associates, Inc.), contract operator of AEDC, AFSC, Arnold Air Force Station, Tennessee. The apparatus was developed under ARO Project No. V32A-15A, and the wind tunnel tests were conducted under ARO Project No. V41A-99A. The manuscript (ARO Control No. ARO-VKF-TR-75-11) was submitted for publication on February 4, 1975.

CONTENTS

| | <u>Page</u> |
|--|-------------|
| 1.0 INTRODUCTION. | 5 |
| 2.0 APPARATUS | |
| 2.1 Model | 5 |
| 2.2 Test Mechanism and Instrumentation | 6 |
| 2.3 Wind Tunnel | 6 |
| 3.0 PROCEDURE AND PRECISION OF DATA | |
| 3.1 Test Conditions | 7 |
| 3.2 Test Procedure | 7 |
| 3.3 Precision of Data | 7 |
| 4.0 RESULTS AND DISCUSSION | 8 |
| 5.0 CONCLUSIONS | 10 |
| REFERENCES | 11 |

ILLUSTRATIONS

Figure

| | |
|---|----|
| 1. Photographs of the Model | |
| a. $\ell/d = 10$ Configuration (Basic Finner) | 13 |
| b. $\ell/d = 15$ Configuration | 13 |
| 2. Model Details | |
| a. $\ell/d = 10$ Configuration (Basic Finner) | 14 |
| b. $\ell/d = 15$ Configuration | 14 |
| 3. VKF 2. G High-Alpha Pitch-Damping Test Mechanism | |
| a. Test Mechanism Details | 15 |
| b. Identification of Sting Pre-Bend Angles | 16 |
| 4. Photographs of Model Installation | |
| a. $\alpha = 72$ deg, $\ell/d = 10$ Configuration (Basic Finner) | 17 |
| b. $\alpha = 0$, $\ell/d = 15$ Configuration | 18 |
| 5. Tunnel A Details | 19 |
| 6. Effect of Sting Configuration on the Stability | |
| Coefficients of the Basic Finner Model | |
| a. $Re_d = 0.086 \times 10^6$ | 20 |
| b. $Re_d = 0.187 \times 10^6$ | 21 |
| c. Comparison of Generated Effective VKF Data with BRL and NSWC Data | 22 |

| <u>Figure</u> | <u>Page</u> |
|--|-------------|
| 7. Dynamic and Static Coefficients as a Function of Angle of Attack for the Basic Finner Model | |
| a. $Re_d = 0.086 \times 10^6$ | 23 |
| b. $Re_d = 0.187 \times 10^6$ | 24 |
| 8. Effects of Apex Angle and Nose Fineness Ratio on the Angle of Attack at Which Unsteadiness in the Crossflow Occurs. | 25 |
| 9. Effect of Reynolds Number on the Stability Coefficients of the Basic Finner Model | 26 |
| 10. Dynamic and Static Stability Coefficients as a Function of Angle of Attack for the $\ell/d = 15$ Configuration | 27 |

TABLES

| | |
|--------------------------------|----|
| 1. Tunnel Conditions | 28 |
| 2. Test Summary | 28 |
| NOMENCLATURE | 29 |

1.0 INTRODUCTION

The current trend in missile development is toward higher fineness ratio configurations (ℓ/d ratios from 12 to 20), low aspect ratio fins, high maneuverability, and high performance. Damping derivatives (pitch, yaw, and roll), especially on slender vehicles with fins, have a strong influence on the vehicle response at extreme maneuver conditions. Theoretical predictions at best apply only at low angles of attack, and since the new missiles are highly maneuverable, large angle-of-attack experimental data are desired for the computerized flight trajectory programs.

A research program was initiated at the Arnold Engineering Development Center (AEDC) von Kármán Gas Dynamics Facility (VKF) for the purpose of developing the capability for obtaining high angle-of-attack pitch-damping data on current missile configurations. A specialized test mechanism consisting of a strut-supported cross-flexure balance capable of testing at angles of attack up to 90 deg at subsonic and supersonic speeds ($M_\infty = 0.2$ to 6) was developed. Wind tunnel verification tests were conducted on two missile configurations at Mach number 2 utilizing the small-amplitude, free-oscillation test technique. Data were obtained at angles of attack from -12 to 86 deg at Reynolds numbers, based on model diameter, of 0.086×10^6 to 0.187×10^6 .

2.0 APPARATUS

2.1 MODEL

The model (Fig. 1), designed and fabricated at VKF, consisted of a stainless steel configuration with an ℓ/d of 10 (commonly referred to as the Basic Finner) and an $\ell/d = 15$ configuration that used a magnesium nose (for ballasting purposes) in conjunction with the Basic Finner aft body and fins. Basically, the model was a 10-deg half-angle cone-cylinder body with four rectangular fins located at the model base. Model diameter was 1.25 in. (one caliber) and the fins had a chord of 0.923 calibers and an overall span of 3 calibers. The moment reference point and model pivot axis were located 6.1 calibers from the model nose for the Basic Finner and 11.1 calibers from the model nose for the $\ell/d = 15$ configuration. Both configurations were balanced to locate

the center of gravity on the flexure pivot axis. The tests were conducted with the model in 45-deg roll orientation for the purpose of comparison with previously obtained experimental data. Model details are shown in Fig. 2.

2.2 TEST MECHANISM AND INSTRUMENTATION

The high-alpha pitch-damping test mechanism, designated VKF 2.G High Alpha (Fig. 3), utilizes a small-amplitude one-degree-of-freedom cross-flexure balance which is supported by a strut and sting that can be manually adjusted to provide minimum aerodynamic interference and angles of attack ranging from -15 to 90 deg. A strain-gage bridge is located on the flexures to provide a voltage proportional to angular displacement. A pneumatic- and spring-operated locking device is provided to hold the model during injection into or retraction from the tunnel. Three balances, having flexure stiffnesses of 2, 3, 23, and 49 in.-lb/deg and maximum amplitudes of ± 4 , ± 3 , and ± 2 deg, respectively, are available for use with the test mechanism. The 49 in.-lb/deg balance was used during the present test. Installation photographs are shown in Fig. 4.

An oscillating-air system was used to displace the model. The driving force was obtained from a high-pressure air supply which was adjusted to the pressure level necessary to overcome the damping moment. The model was oscillated by two air jets (Fig. 3a) that were regulated by a remotely controlled servovalve oscillating at the natural frequency of the model and balance system. The driving force could be stopped abruptly by a solenoid valve and data recorded as the amplitude decreased.

2.3 WIND TUNNEL

Supersonic Wind Tunnel (A) in VKF is a continuous, closed-circuit, variable density wind tunnel with an automatically driven flexible-plate-type nozzle and a 40- by 40-in. test section. The tunnel can be operated at Mach numbers from 1.5 to 6 at maximum stagnation pressure from 29 to 200 psia, respectively, and at stagnation temperatures up to 750°R. Minimum stagnation pressures range from about one-tenth to one-twentieth of the maximum pressure at each Mach number. Tunnel A is equipped with a model injection system, which allows removal

of the model from the test section while the tunnel remains in operation. Tunnel details are shown in Fig. 5.

3.0 PROCEDURE AND PRECISION OF DATA

3.1 TEST CONDITIONS

The nominal wind tunnel test parameters at which the data were obtained are presented in Table 1, and summaries of the test configurations are presented in Table 2. Data were normally obtained for oscillation amplitudes from ± 1.4 to ± 0.6 deg. The data are presented for oscillation amplitudes (θ) of ± 1 deg.

3.2 TEST PROCEDURE

The test procedure was to set the forcing air pressure to a sufficiently high value, open the solenoid valve, adjust the frequency of the servovalve to the natural frequency of the model-balance system, and then, when the model amplitude reached the desired value, close the solenoid valve. The switch that closed the valve also started the high-speed scanner which read the digitized displacement signal onto magnetic tape for data reduction. Data reduction was accomplished by the logarithm decrement method described in Ref. 1.

3.3 PRECISION OF DATA

3.3.1 Tunnel Conditions

Uncertainties (bands which include 95 percent of the calibration data) in the basic tunnel parameters (p_o , T_o , and M_∞) were estimated from repeat calibrations of the instrumentation and from repeatability and uniformity of the test section flow during tunnel calibrations. These uncertainties were used to estimate uncertainties in other free-stream properties using a Taylor series method of error propagation (Ref. 2). The estimated uncertainties are as follows:

| $Re_d \times 10^{-6}$ | Uncertainty, percent | | | |
|-----------------------|-------------------------------------|-----------------------------|-------------------------------------|-------------------------------------|
| | $\frac{\Delta(M_\infty)}{M_\infty}$ | $\frac{\Delta(Re_d)}{Re_d}$ | $\frac{\Delta(q_\infty)}{q_\infty}$ | $\frac{\Delta(V_\infty)}{V_\infty}$ |
| 0.086 | 0.5 | 0.9 | 0.8 | 0.3 |
| 0.187 | 0.5 | 0.7 | 0.6 | 0.3 |

3.3.2 Aerodynamic Coefficients

The balance was calibrated before and after the test, and check calibrations were made during the test. In addition, structural damping values were obtained at vacuum conditions before the tunnel entry to evaluate the still-air damping contribution. The uncertainties in the balance and data system were combined with uncertainties in the tunnel parameters assuming a Taylor series error propagation (Ref. 2) to estimate the precision of the aerodynamic coefficients. The estimated uncertainties are as follows:

| Configuration | $Re_d \times 10^{-6}$ | $C_{m_q} + C_{m_{\dot{\alpha}}}$ | $\Delta(C_{m_q} + C_{m_{\dot{\alpha}}})$ | $C_{m_{\alpha}}$ | $\Delta(C_{m_{\alpha}})$ | C_m | $\Delta(C_m)$ |
|------------------------------|-----------------------|----------------------------------|--|------------------|--------------------------|-------|---------------|
| $l/d = 10$ (Basic Finner) | 0.086 | -100 | ± 20 | -25 | ± 2.2 | -2 | ± 0.26 |
| | | -200 | ± 22 | -15 | | -4 | ± 0.26 |
| | | -400 | ± 25 | -5 | | -6 | ± 0.27 |
| | | -600 | ± 28 | 5 | | -8 | ± 0.27 |
| | | -700 | ± 30 | 10 | | -10 | ± 0.27 |
| | 0.187 | -100 | ± 10 | -25 | ± 1.1 | -2 | ± 0.13 |
| | | -200 | ± 12 | -15 | | -4 | ± 0.13 |
| | | -400 | ± 15 | -5 | | -6 | ± 0.13 |
| | | -600 | ± 19 | 5 | | -8 | ± 0.13 |
| | | -700 | ± 21 | 10 | | -10 | ± 0.14 |
| $l/d = 15$ | 0.086 | -200 | ± 24 | -5 | ± 2.2 | 4 | ± 0.26 |
| | | -400 | ± 26 | 10 | | 8 | ± 0.27 |
| | | -800 | ± 32 | 20 | | 12 | ± 0.28 |
| | | -1200 | ± 38 | 30 | | 16 | ± 0.29 |
| | | -1600 | ± 45 | 40 | | 20 | ± 0.31 |
| | 0.187 | -400 | ± 15 | -5 | ± 1.1 | 4 | ± 0.13 |
| | | -800 | ± 22 | 20 | | --- | --- |
| | | -1200 | ± 29 | 40 | | --- | --- |
| | | | | | | | |
| | | | | | | | |

4.0 RESULTS AND DISCUSSION

The damping derivatives, static stability derivatives and pitching-moment coefficients are presented in Fig. 6 as a function of angle of attack for the $l/d = 10$ configuration (Basic Finner) for Reynolds numbers, based on model diameter, of 0.086×10^6 and 0.187×10^6 . The different symbols in Fig. 6 indicate the data that were obtained with one particular strut and support sting arrangement. In general the data overlap from the different strut-sting combinations was good for both the static and dynamic measurements. The fact that the data overlap was good gives a high confidence level that the strut-support sting interference was not appreciable for angles of attack greater than 6 deg, where data overlap started (Fig. 6b). The possibility

existed at low angles of attack that the strut would cause interference until the angle of attack was sufficient to hide the strut behind the model. However, the interference, if existing, appeared to be a minimum since the pitch-damping and static stability data were fairly symmetrical about $\alpha = 0$ and also showed fairly good agreement at $\alpha = 0$ with data free of any support effects (BRL, Ref. 3) and with transverse rod support data (NSWC, Ref. 4) (Fig. 6a and b). The present data are small-amplitude, local-effective derivatives (Ref. 5), whereas the BRL and NSWC data are large-amplitude effective data. In order that all the data being compared be effective values, the technique of Billingsley and Norman (Ref. 6) was used to generate effective derivatives from the present experimental data (local-effective). The results are shown in Fig. 6c with the BRL and NSWC data showing fairly good agreement with the generated effective derivatives, considering the differences in test conditions, test techniques, etc.

The data in Fig. 6 are shown again in Fig. 7 using just one symbol for clarity. Analysis of the data in Fig. 7 showed both the dynamic and static coefficients to be a highly non-linear function of angle of attack. It is of interest to note that for angles of attack above 40 deg at the higher Reynolds number, $Re_d = 0.187 \times 10^6$ (Fig. 7b), the dynamic measurements exhibited more scatter as compared to lower α data, and the damping derivatives also became highly nonlinear and oscillatory. A possible explanation for this unsteady dynamic data is an unsteady vortex system and/or the interaction between the shed vortices and fins. It is documented by Gowen and Perkins (Ref. 7) that as the angle of attack is increased, the vortex system on the leeward side changes from a steady symmetric pair to a steady asymmetric configuration of two or more vortices and then to an unsteady asymmetric system at the high angles of attack. Gowen and Perkins (Ref. 7) were also able to obtain a correlation for several models defining the region of unsteady wake flow as a function of nose fineness ratio and apex angle. The correlation is shown in Fig. 8 with the conditions of the Basic Finner model. According to the correlation the borderline to the unsteady conditions begins at $\alpha \approx 35$ deg for the Basic Finner model. This seems to be in agreement with the beginning of the unsteady data in Fig. 7b. In addition, the repeatability of the high α damping measurements at the lower Reynolds number (Fig. 7a) was found to be better than that at the larger Reynolds number (Fig. 7b). Normally the reverse of this is true since the measured damping moment is larger at the higher Reynolds number (see uncertainty values, Section 3.3.2). The answer to this may be that the unsteadiness of the vortices may be more pronounced at the higher Reynolds number.

Figure 9 shows the comparison of the Basic Finner data for the two Reynolds numbers tested. As mentioned in the previous paragraph, there were some small Reynolds number effects at the high angles of attack which were pertinent in analysing the unsteady nonlinear damping data; however, over the angle-of-attack range (except at $\alpha \approx 80$ deg) there were essentially no consistent effects of Reynolds number for the limited Reynolds number range investigated. At $\alpha \approx 80$ deg, model damping decreased sharply for both Reynolds numbers. The lower Reynolds number ($Re_d = 0.086 \times 10^6$) data actually showed the model to be slightly unstable. However, model damping on each side of this "instantaneous peak" was quite high. The static stability derivative (C_{m_α}) also shows a spike at $\alpha \approx 80$ deg for both Reynolds numbers.

The static and dynamic data for the $l/d = 15$ configuration are presented in Fig. 10 for both Reynolds numbers tested. Data were obtained only up to $\alpha = 31$ deg because of balance limitation in pitching moment. The aft pivot axis (center of gravity) location produced large positive pitching moments as evidenced by the unstable static data (C_{m_α} and C_m). For the α range tested, the $l/d = 15$ configuration produces about the same damping trends as the $l/d = 10$ configuration; however, the damping levels are generally much higher for the longer configuration.

5.0 CONCLUSIONS

Wind tunnel tests were conducted to evaluate a newly developed high angle-of-attack missile test mechanism. Data were obtained at $M_\infty = 1.96$ at angles of attack from -12 to 86 deg for Reynolds numbers, based on model diameter, of 0.086×10^6 and 0.187×10^6 . Two missile configurations having length-to-diameter ratios of 10 and 15 were tested. Conclusions based on the results presented in this report are given below.

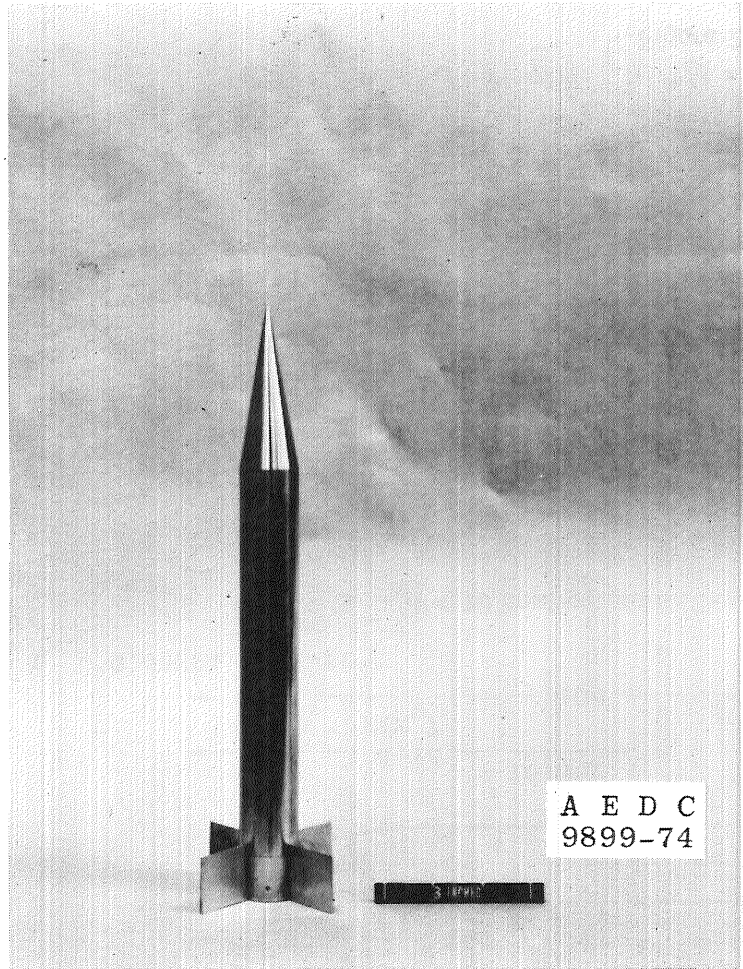
1. The pitch-damping derivatives, the slope of the pitching-moment curve, and the pitching-moment coefficient can be measured accurately at angles of attack up to 90 deg by the high α missile test mechanism. Strut interference, if existent, is not appreciable.
2. The pitch-damping derivatives, the slope of the pitching-moment curve, and pitching-moment coefficients were

found to be nonlinear functions of angle of attack and except for one "instantaneous peak" at $\alpha \approx 80$ deg, both configurations are dynamically stable.

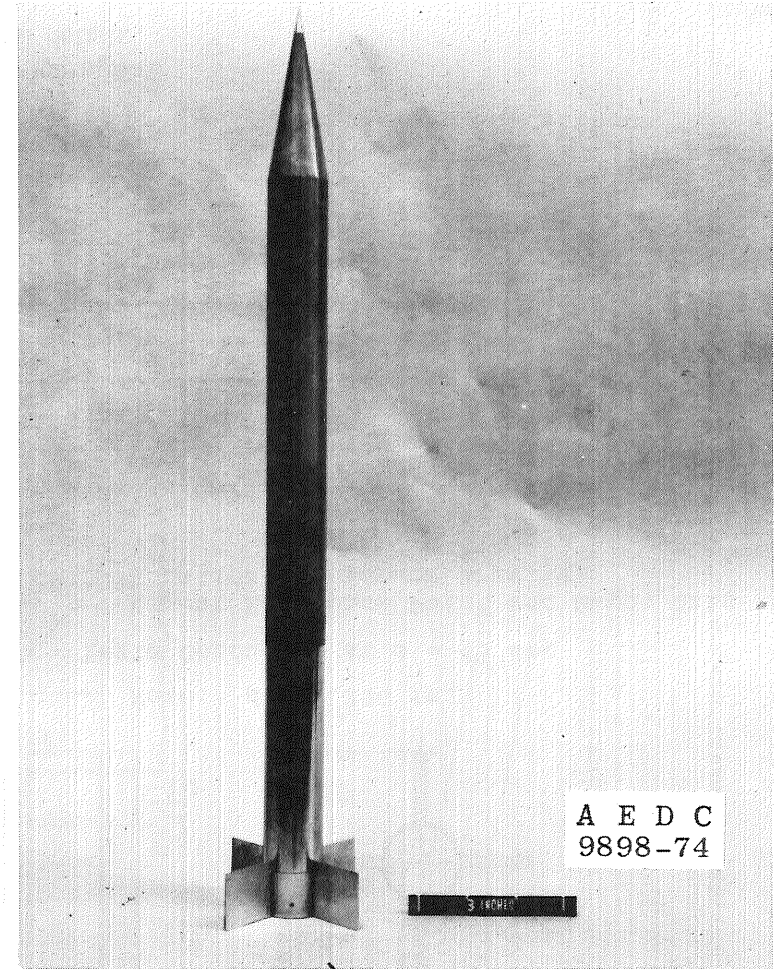
3. Previously published data taken at low angles of attack are in satisfactory agreement with the present results, considering differences in test conditions.

REFERENCES

1. Schueler, C. J., Ward, L. K., and Hodapp, A. E., Jr. "Techniques for Measurement of Dynamic Stability Derivatives in Ground Test Facilities." AGARDograph 121 (AD669227), October 1967.
2. Beers, Yardley. Introduction to the Theory of Error. Addison Wesley Publishing Co., Inc., Reading, Mass., 1957, pp. 26-36. (Second Edition).
3. MacAllister, L. C. "The Aerodynamic Properties of a Simple Non-Rolling Finned Cone-Cylinder Configuration Between Mach Numbers 1.0 and 2.5." BRL Report 934, May 1955.
4. Shantz, Irving and Groves, Robert T. "Dynamic and Static Stability Measurements of the Basic Finner at Supersonic Speeds." NAVORD Report 4516, January 1960.
5. Uselton, James C. and Uselton, B. L. "A Look at the Validity of the Small Amplitude Oscillation Dynamic-Stability Measurement Technique." AIAA Paper No. 75-211, Presented at the AIAA 13th Aerospace Sciences Meeting, January 1975.
6. Billingsley, J. P. and Norman, W. S. "Relationship Between Local and Effective Aerodynamic Pitch-Damping Derivatives as Measured by a Forced-Oscillation Balance for Preliminary Viking Configurations." AEDC-TR-72-25 (AD741769), May 1972.
7. Gowen, Forrest E. and Perkins, Edward W. "A Study of the Effects of Body Shape on the Vortex Wakes of Inclined Bodies at a Mach Number of 2." NACA RM A53I17, December 1953.

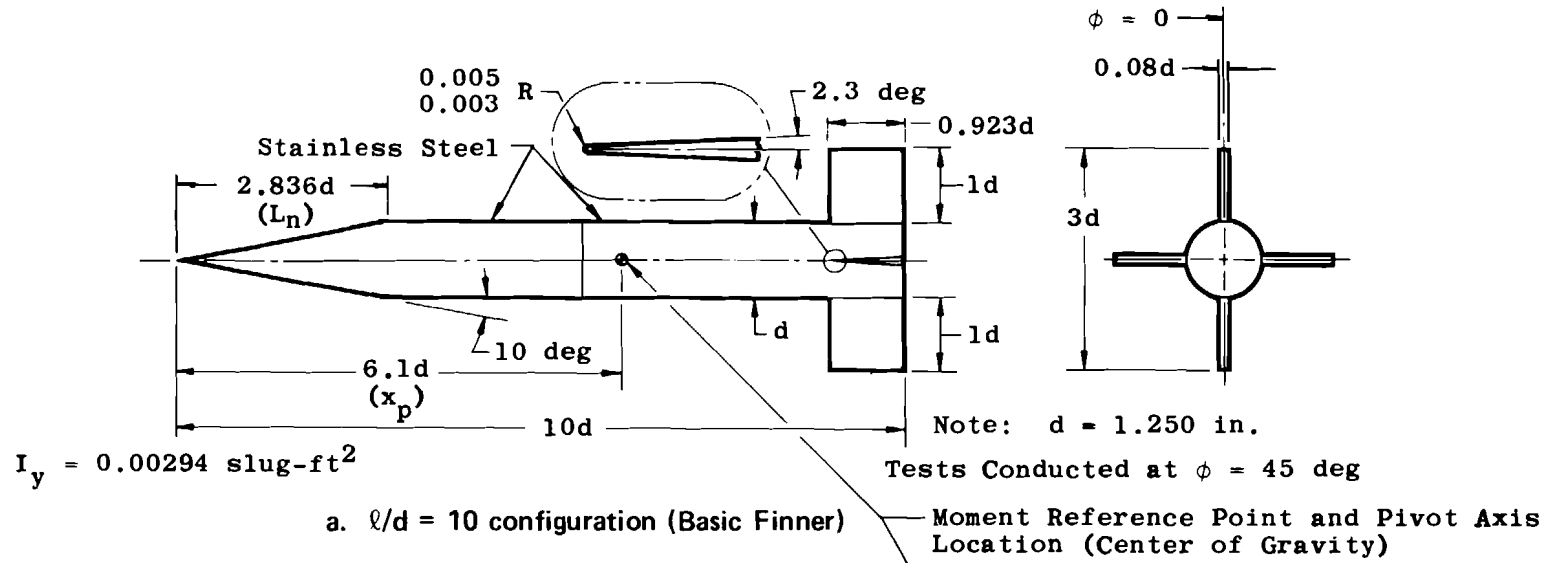


a. $l/d = 10$ configuration (Basic Finner)

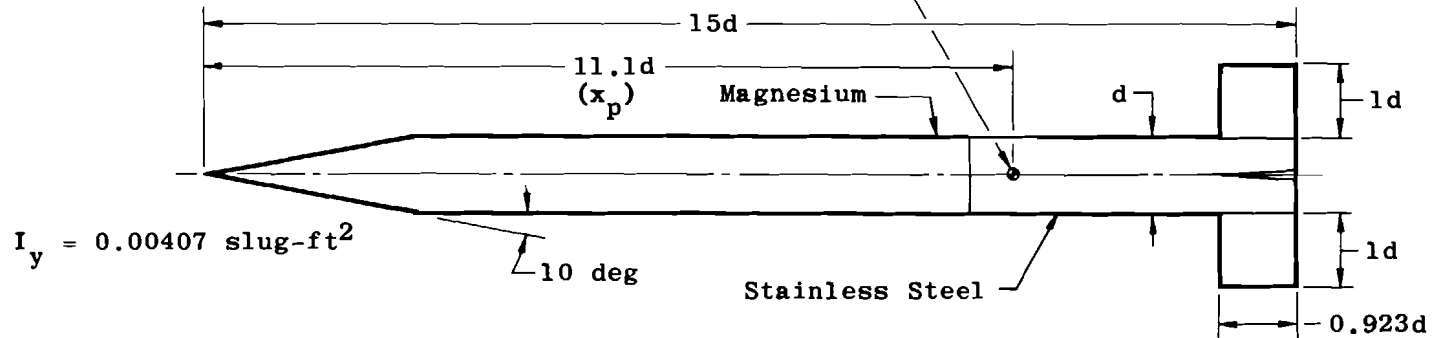


b. $l/d = 15$ configuration

Figure 1. Photographs of the model.

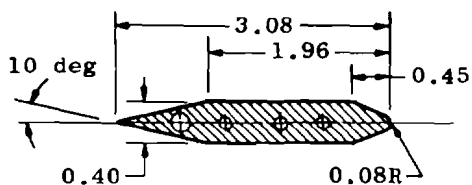
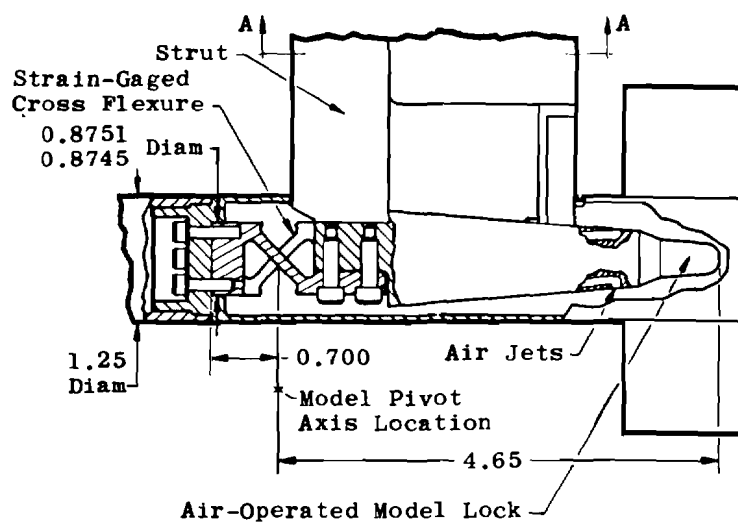
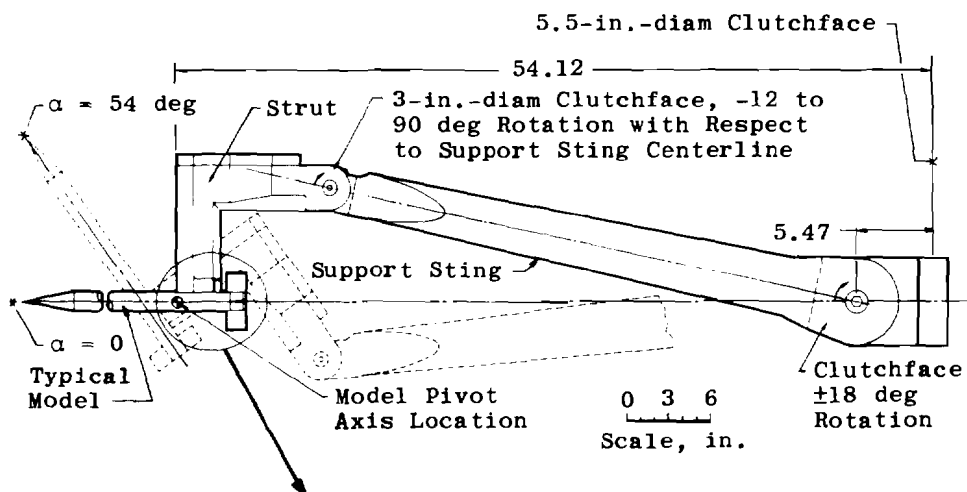


a. $\ell/d = 10$ configuration (Basic Finner)



Dimensions in Calibers

b. $\ell/d = 15$ configuration
Figure 2. Model details.

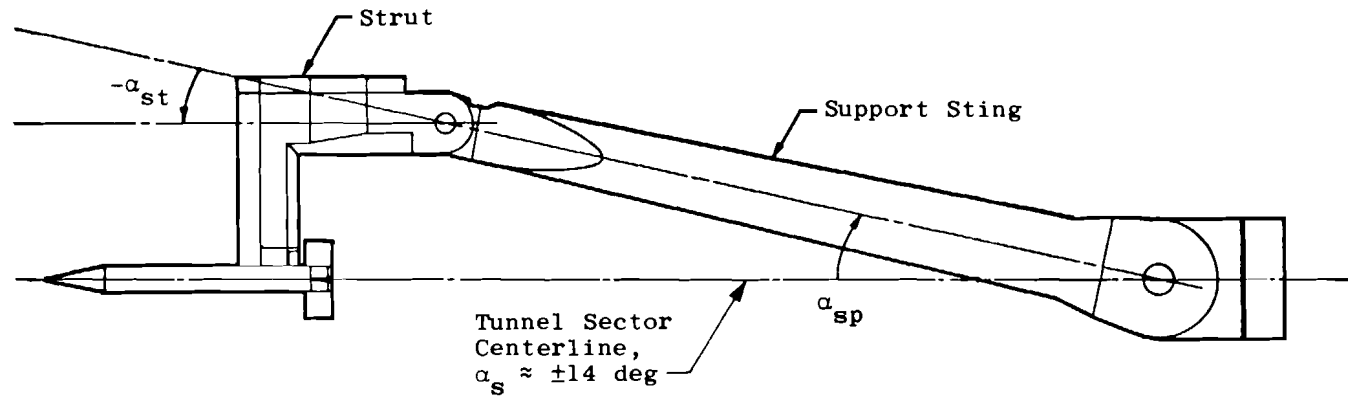


Section A-A

Dimensions in Inches

a. Test mechanism details

Figure 3. VKF 2.G high-alpha pitch-damping test mechanism.



α_{sp} - Angle of Support Sting with Respect to Centerline of Tunnel Sector, deg

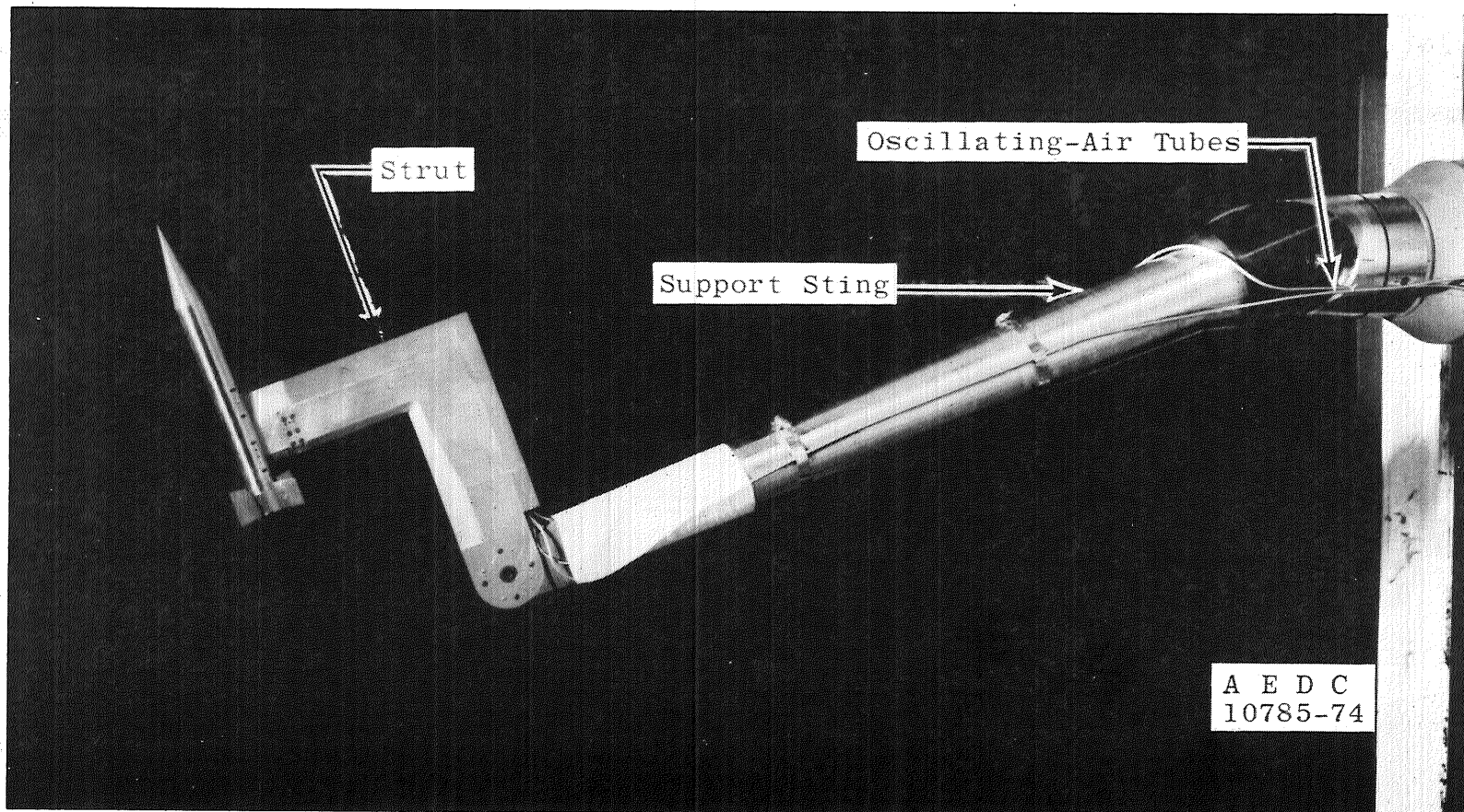
α_{st} - Angle of Strut with Respect to Support Sting Centerline, deg

α_s - Tunnel Sector Pitch Angle, deg

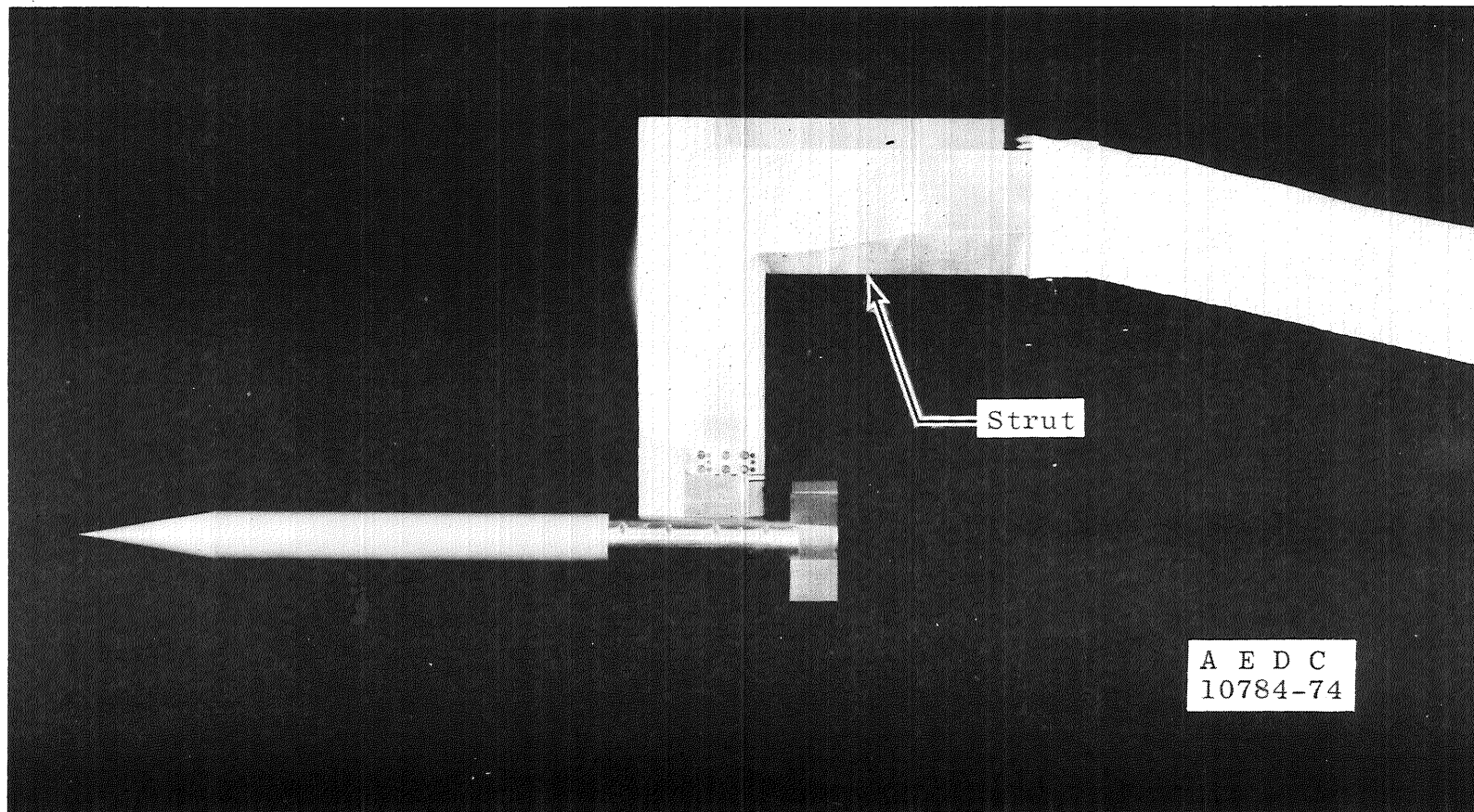
α_{pb} - Effective Sting Pre-Bend, deg ($\alpha_{pb} = \alpha_{sp} + \alpha_{st}$)

$\alpha = \alpha_s + \alpha_{pb} + \alpha_{trim}$

b. Identification of sting pre-bend angles
Figure 3. Concluded.



a. $\alpha = 72$ deg, $l/d = 10$ configuration (Basic Finner)
 Figure 4. Photographs of model installation.



b. $a = 0$, $\ell/d = 15$ configuration
Figure 4. Concluded.

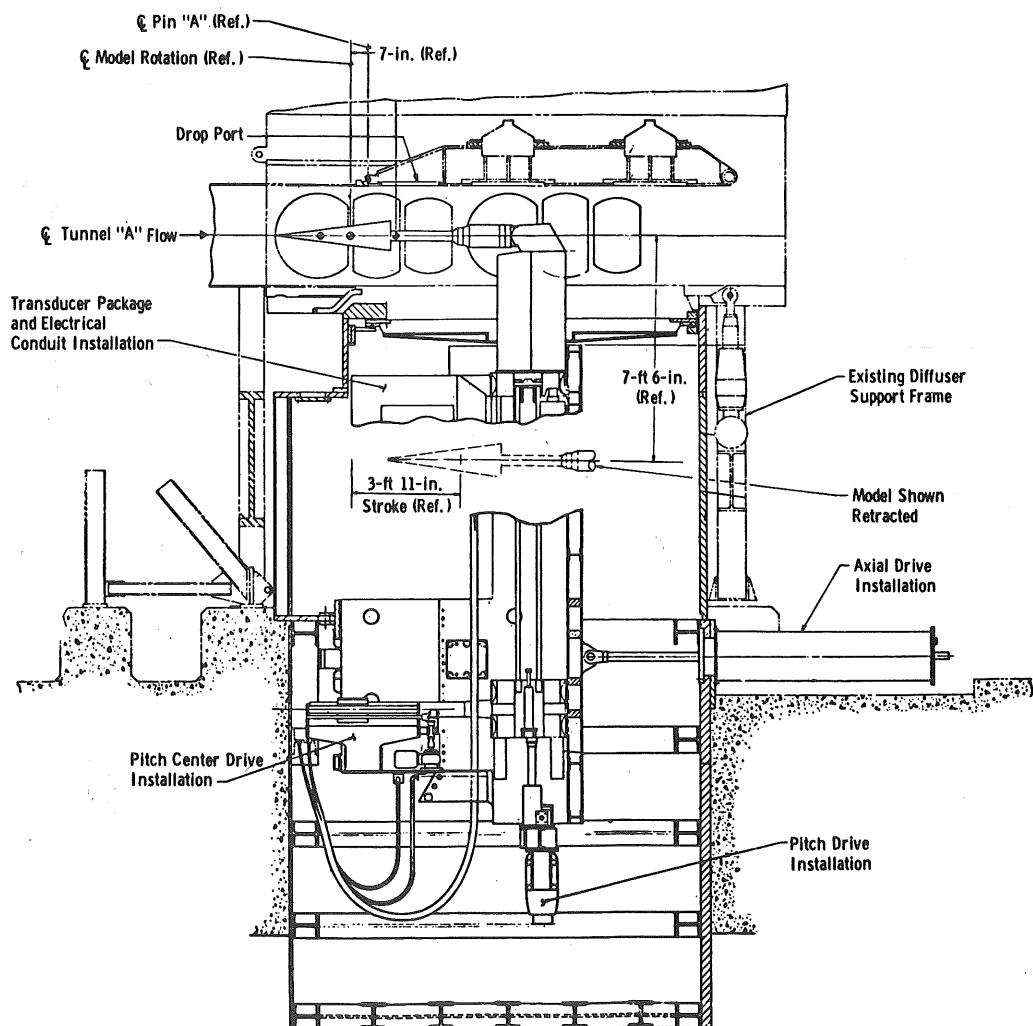
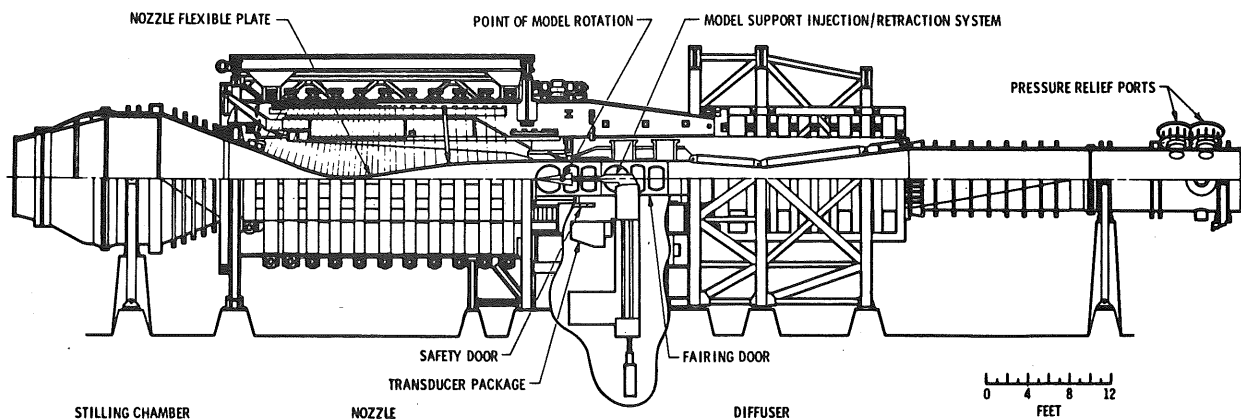


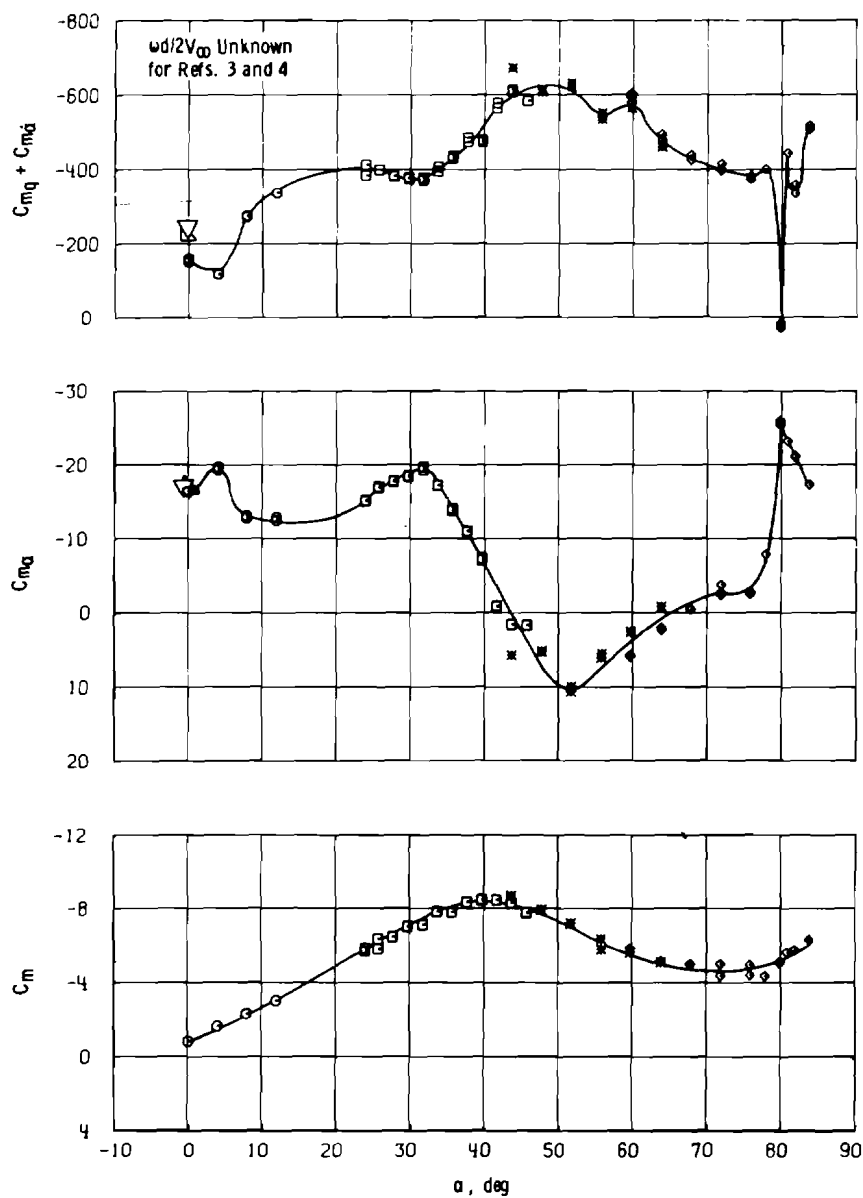
Figure 5. Tunnel A details.

| Sym | α_{st}, deg | α_{sp}, deg | α_{pb}, deg |
|-----|---------------------------|---------------------------|---------------------------|
| ● | -12 | 12 | 0 |
| □ | 36 | 0 | 36 |
| * | 60 | -6 | 54 |
| ◇ | 90 | -18 | 72 |

Strut Support, $M_\infty = 1.96$, $\beta = 45 \text{ deg}$,
 $\theta = \pm 1 \text{ deg}$, $\omega d/2V_\infty = 0.0086$,
 $x_p/d = 6.1$, $z/d = 10$

▽ BRL (Ref. 3) $M_\infty = 2.05$, $x_p/d = 6.1$, Range Data, No Support, $\beta_{\text{launch}} = 45 \text{ deg}$,
 $\theta \approx \pm 3 \text{ deg}$

△ NSWC (Ref. 4) $M_\infty = 2.16$, $Re_d = 0.45 \times 10^6$, $x_p/d = 6.0$, $\theta \approx \pm 4 \text{ deg}$,
 $\beta = 45 \text{ deg}$, Transverse Rod Support



a. $Re_d = 0.086 \times 10^6$

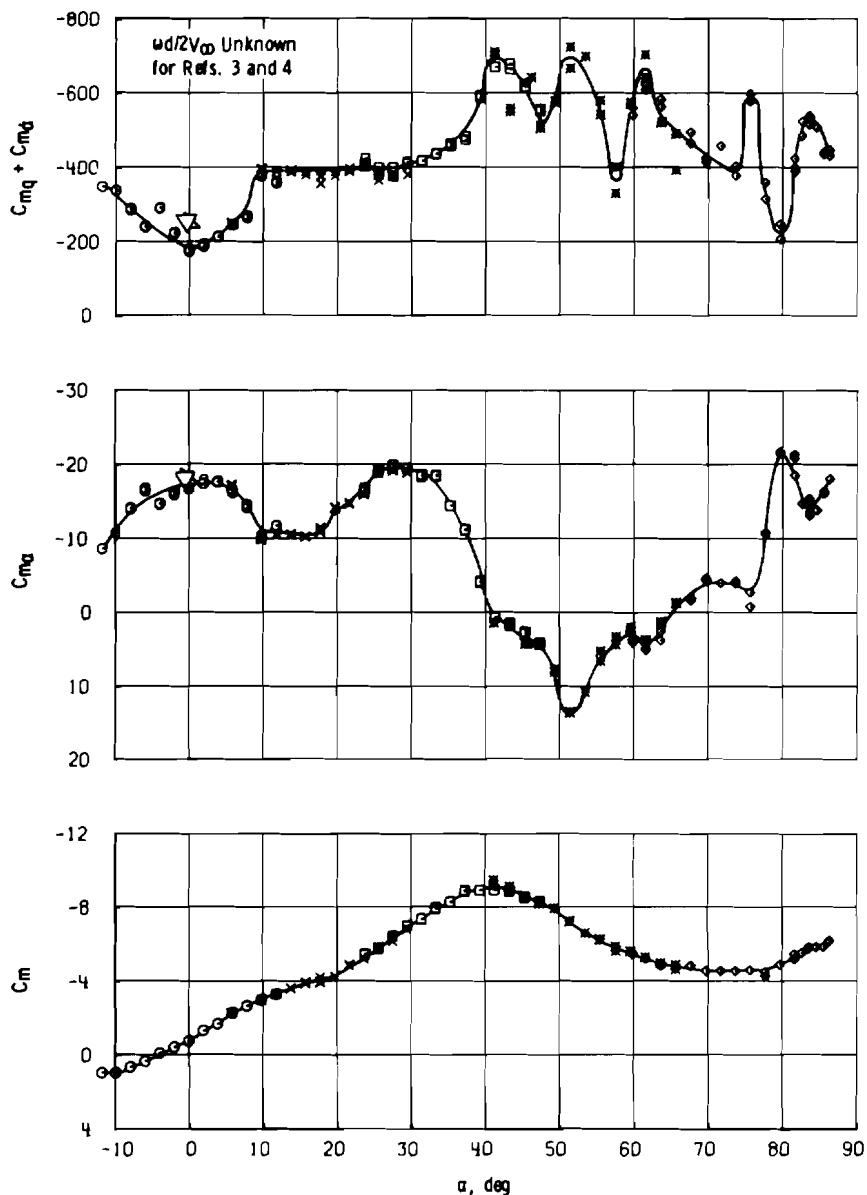
Figure 6. Effect of sting configuration on the stability coefficients of the Basic Finner model.

| Sym | α_{st}, deg | α_{sp}, deg | α_{pb}, deg |
|-----|---------------------------|---------------------------|---------------------------|
| ○ | -12 | 12 | 0 |
| × | 12 | 6 | 18 |
| □ | 36 | 0 | 36 |
| ■ | 60 | -6 | 54 |
| ◇ | 90 | -18 | 72 |

Strut Support, $M_\infty = 1.96$, $\theta = 45 \text{ deg}$,
 $\theta = \pm 1 \text{ deg}$, $\omega d/2V_\infty = 0.0067$,
 $x_p/d = 6.1$, $z/d = 10$

▽ BRL (Ref. 3) $M_\infty = 2.05$, $x_p/d = 6.1$, Range Data, No Support, $\theta_{\text{launch}} = 45 \text{ deg}$,
 $\theta \approx \pm 3 \text{ deg}$

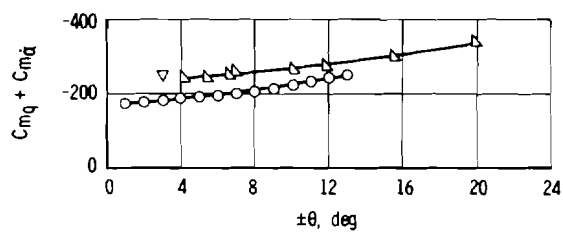
△ NSWC (Ref. 4) $M_\infty = 2.16$, $Re_d = 0.45 \times 10^6$, $x_p/d = 6.0$, $\theta \approx \pm 4 \text{ deg}$,
 $\theta = 45 \text{ deg}$, Transverse Rod Support



b. $Re_d = 0.187 \times 10^6$
 Figure 6. Continued.

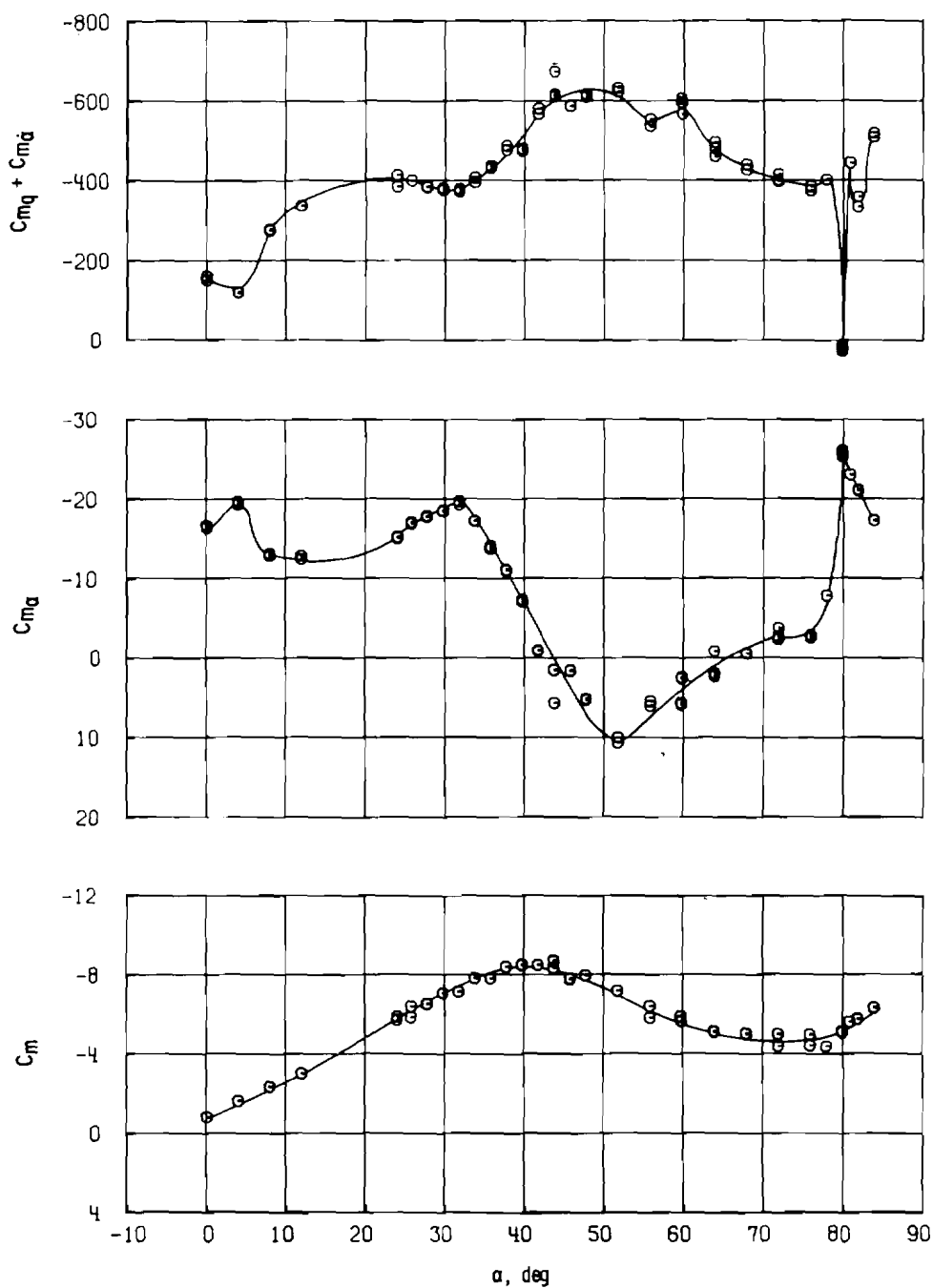
| Sym | Facility | Model Support | Type Data |
|-----|---------------|--------------------|---------------------|
| ○ | VKF | Strut | Generated Effective |
| ▽ | BRL (Ref. 3) | None (Free Flight) | Effective |
| △ | NSWC (Ref. 4) | Transverse Rod | Effective |

| Sym | $Re_d \times 10^{-6}$ | $\omega d/2V_\infty$ | x_p/d | ϕ , deg | α , deg |
|-----|-----------------------|----------------------|---------|--------------|----------------|
| ○ | 0.187 | 0.0087 | 6.1 | 45 | 0 |
| ▽ | Unknown | Unknown | 6.1 | 45 (Launch) | 0 |
| △ | 0.45 | Unknown | 6.0 | 45 | 0 |



- c. Comparison of generated effective VKF data with BRL and NSWC data
Figure 6. Concluded.

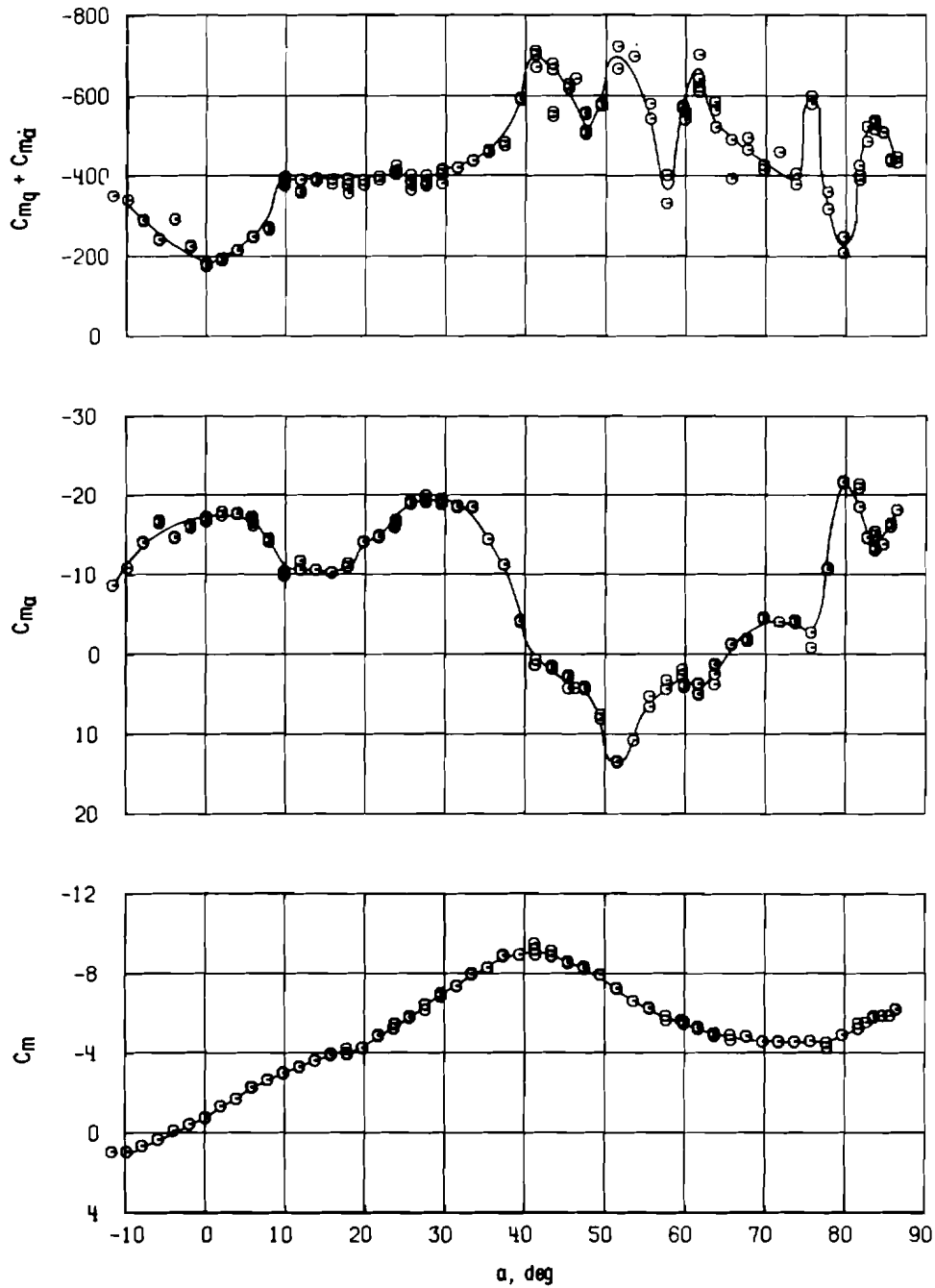
$l/d = 10$ $M_\infty = 1.96$, $\theta = \pm 1$ deg
 $x_p/d = 6.1$ $\omega d/2V_\infty = 0.0086$
 $\phi = 45$ deg



a. $Re_d = 0.086 \times 10^6$

Figure 7. Dynamic and static coefficients as a function of angle of attack for the Basic Finner model.

$l/d = 10$ $M_\infty = 1.96$, $\theta = \pm 1$ deg
 $x_p/d = 6.1$ $wd/2V_\infty = 0.0087$
 $\phi = 45$ deg



b. $Re_d = 0.187 \times 10^6$
Figure 7. Concluded.

Note: This figure was extracted from Ref. 7.

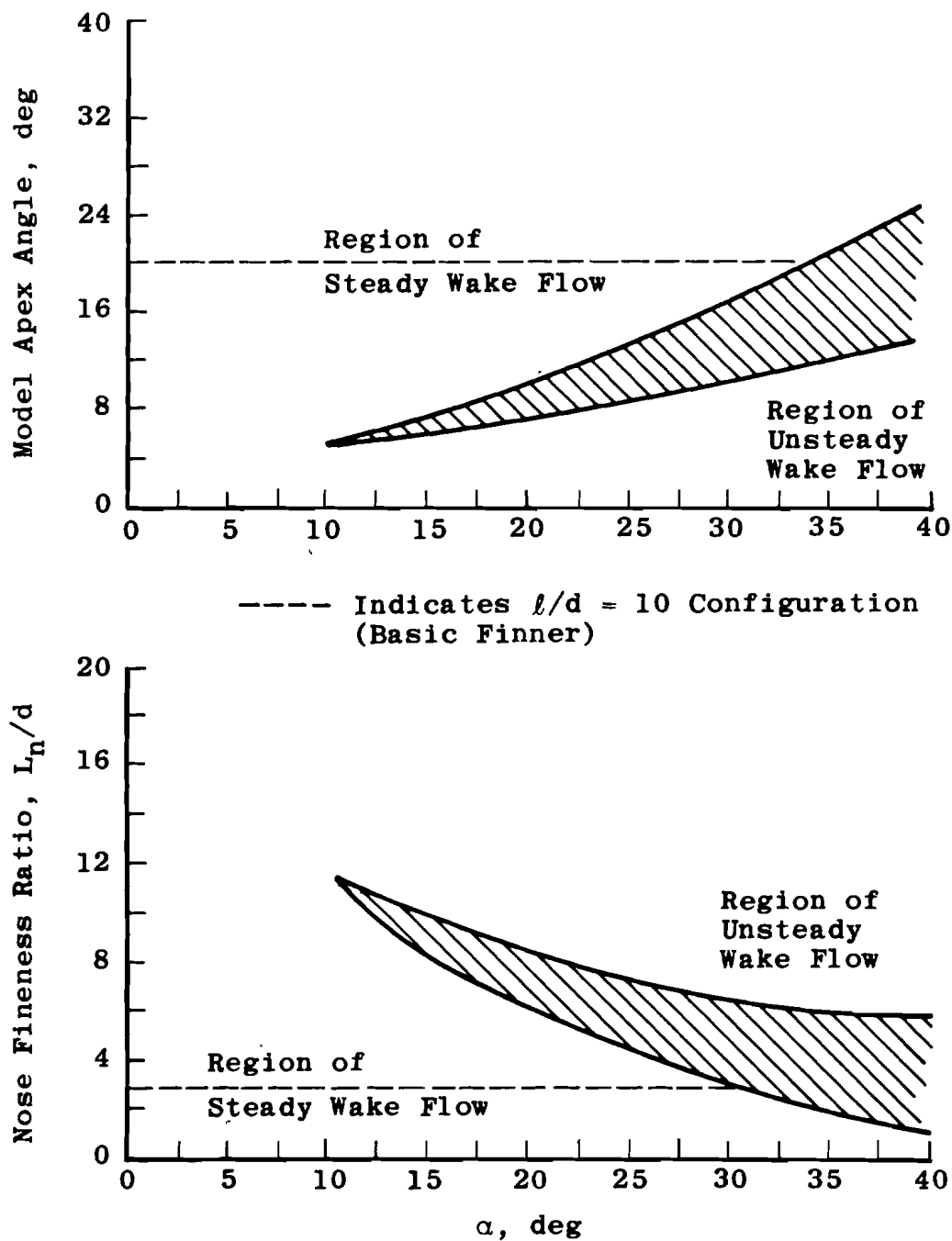


Figure 8. Effects of apex angle and nose fineness ratio on the angle of attack at which unsteadiness in the crossflow occurs.

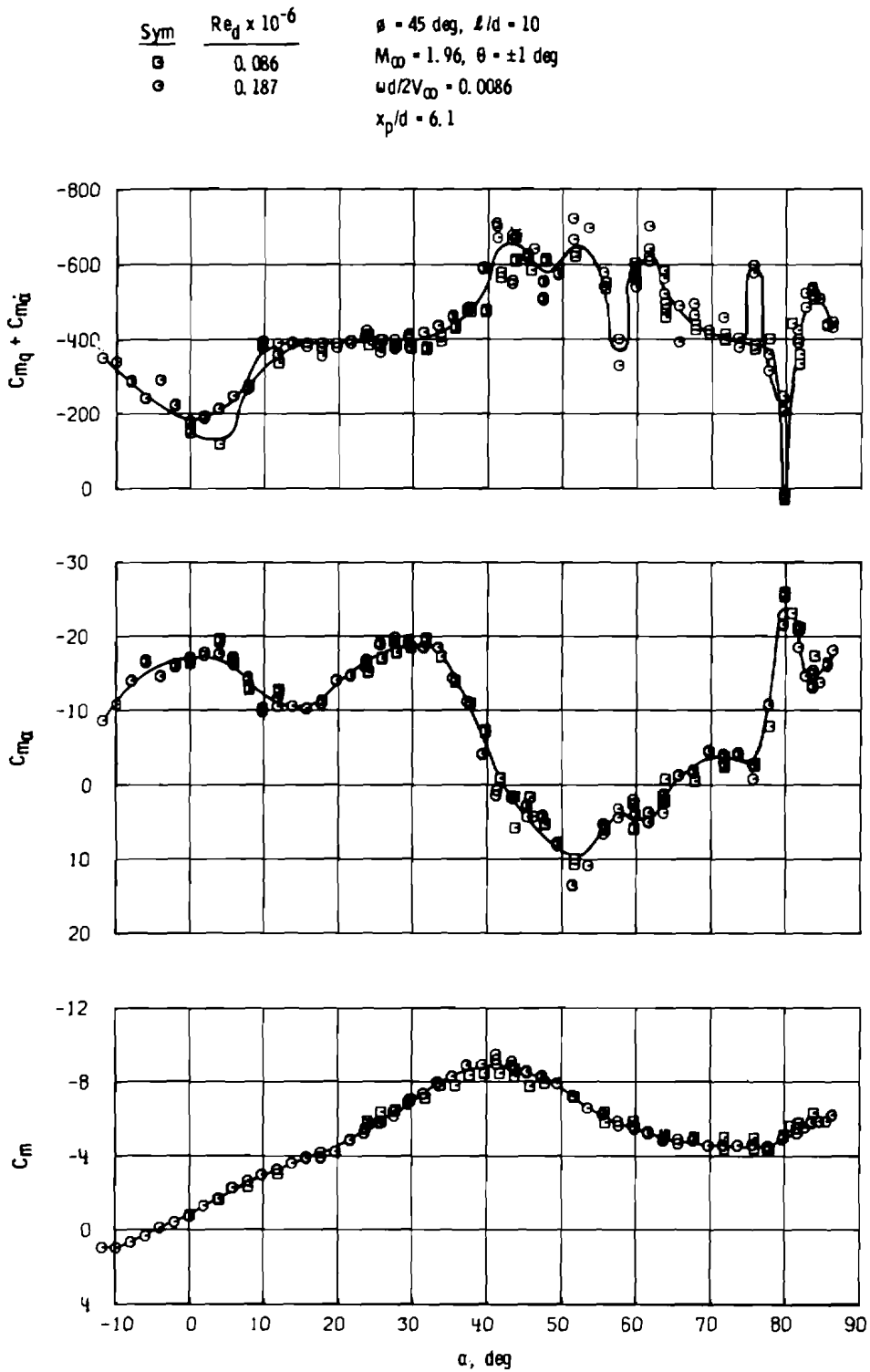


Figure 9. Effect of Reynolds number on the stability coefficients of the Basic Finner model.

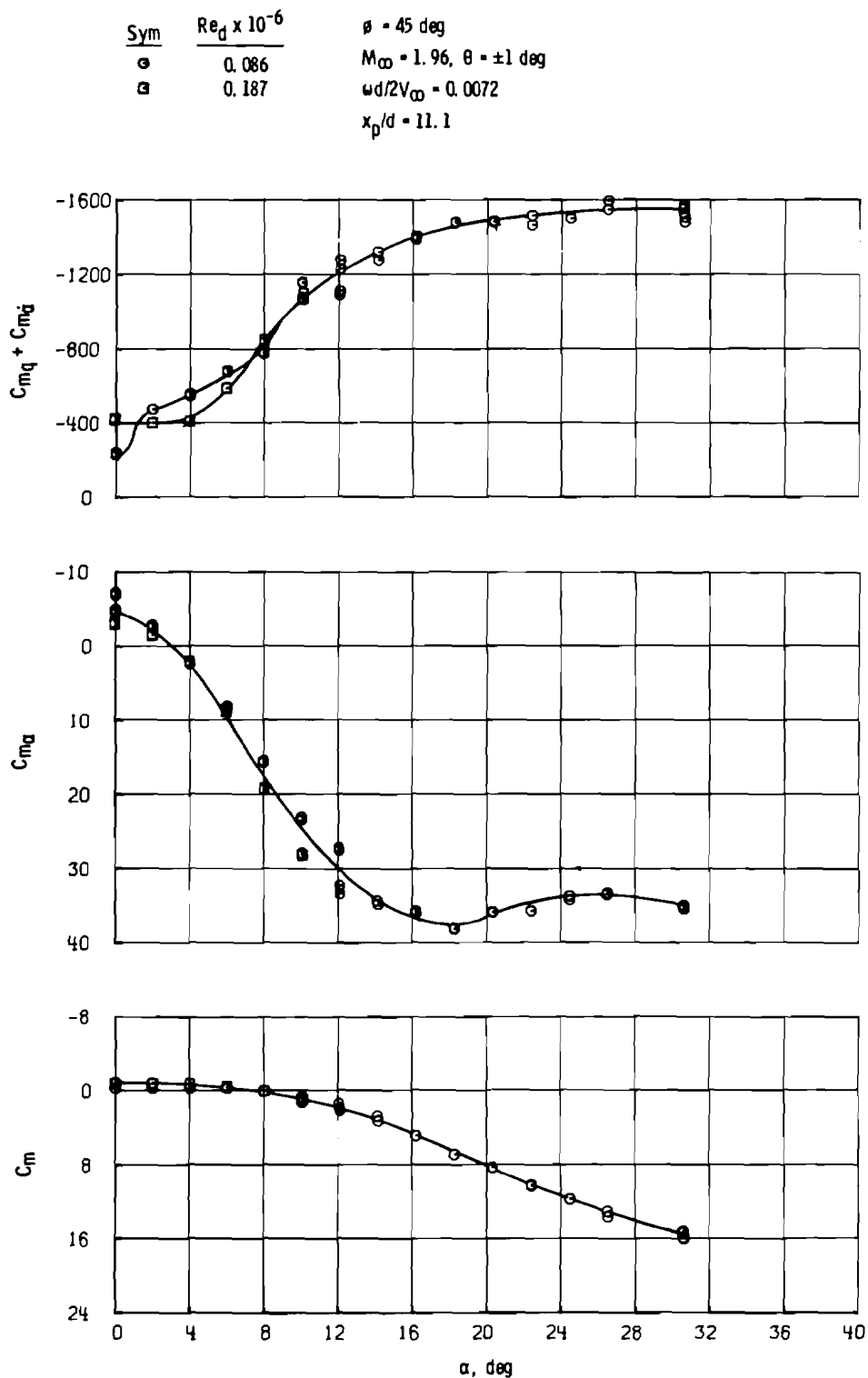


Figure 10. Dynamic and static-stability coefficients as a function of angle of attack for the $l/d = 15$ configuration.

Table 1. Tunnel Conditions

| Test Condition | M_∞ | $Re_d \times 10^{-6}$ | p_o , psia | T_o , °R | q_∞ , psia | V_∞ , ft/sec |
|-------------------|------------|-----------------------|-----------------|---------------|----------------------|------------------------|
| A | 1.96 | 0.086 | 3.30 | 551 | 1.21 | 1696 |
| B | 1.96 | 0.187 | 7.10 | 552 | 2.59 | 1698 |

Table 2. Test Summary

| Configuration | Test Condition* | $\omega d / 2V_\infty \times 10^3$ | α , deg |
|---------------|--------------------|------------------------------------|-------------------|
| $l/d = 10$ | A | 8.7 | 0 to 84 |
| | B | 8.7 | -12 to 86 |
| $l/d = 15$ | A | 7.3 | 0 to 35 |
| | B | 7.3 | 0 to 10 |

*As defined in Table 1.

NOMENCLATURE

| | |
|---------------------|---|
| A | Reference area ($\pi d^2/4$), 0.008522 ft ² |
| C_m | Pitching-moment coefficient, pitching moment/ $q_\infty Ad$ |
| C_{mq} | Pitching-moment coefficient due to pitch velocity, $\partial(C_m)/\partial(qd/2V_\infty)$, radian ⁻¹ |
| $C_{m\alpha}$ | Pitching-moment coefficient due to angle of attack, $\partial C_m/\partial\alpha$, radian ⁻¹ |
| $C_{m\dot{\alpha}}$ | Pitching-moment coefficient due to rate of change of angle of attack, $\partial(C_m)/\partial(\dot{\alpha}d/2V_\infty)$, radian ⁻¹ |
| d | Reference length (model diameter), 0.10417 ft |
| I_y | Model moment of inertia about pitch axis, slug-ft ² |
| L_n | Length of conical forebody nose, in. |
| ℓ | Model length, ft |
| M_∞ | Free-stream Mach number |
| p_o | Tunnel stilling chamber pressure, psia |
| q | Pitching velocity, radians/sec |
| q_∞ | Free-stream dynamic pressure, psia or psfa |
| Re_d | Free-stream Reynolds number based on model diameter (d) |
| T_o | Tunnel stilling chamber temperature, °R |
| V_∞ | Free-stream velocity, ft/sec |
| x_p | Distance from model nose to pivot axis (center of gravity), in. |
| α | Angle of attack, deg, $\alpha = \alpha_s + \alpha_{pb} + \alpha_{trim}$ |

| | |
|----------------------|--|
| α_{pb} | Effective sting pre-bend, deg, $\alpha_{pb} = \alpha_{sp} + \alpha_{st}$ |
| α_s | Tunnel sector pitch angle, deg |
| α_{sp} | Angle of support sting with respect to centerline of tunnel sector, deg |
| α_{st} | Angle of strut with respect to support sting centerline, deg |
| α_{trim} | Angular deflection of cross-flexure balance because of static pitching moment, deg |
| $\dot{\alpha}$ | Time rate of change of angle of attack, radians/sec |
| $\Delta()$ | Uncertainty (95-percent confidence limit) |
| θ | Oscillation amplitude, deg |
| ϕ | Model roll angle, deg |
| ω | Angular frequency, radians/sec |
| $\omega d/2V_\infty$ | Reduced frequency parameter, radians |